JACS
JOURNAL OF THE AMERICAN CHEMICAL SOCIETY
Article
pubs.acs.org/JACS

Pyrene-Edged $Fe^{II}_4L_6$ Cages Adaptively Reconfigure During Guest Binding

Tanya K. Ronson,[†] Aaron B. League,[‡] Laura Gagliardi,[‡] Christopher J. Cramer,[‡] and Jonathan R. Nitschke*,[†]

[†]Department of Chemistry, University of Cambridge, Lensfield Road, Cambridge CB2 1EW, United Kingdom

[‡]Department of Chemistry, Chemical Theory Center, and Supercomputing Institute, University of Minnesota, 207 Pleasant Street SE, Minneapolis, Minnesota 55455, United States

Supporting Information

ABSTRACT: Differential guest-binding behavior was observed between two pyrene-edged Fe_4L_6 cages, prepared from isomeric bis(4-aminophenyl)pyrene derivatives, 2-formylpyridine and iron(II). The cage based on a 1,6-pyrene scaffold possesses an enclosed cavity suitable for the encapsulation of large hydrophobic guests including fullerenes, polycyclic aromatic hydrocarbons, and large, structurally complex natural products such as steroids. Addition of the fullerenes C_{60} and C_{70} to the cage brought about a re-equilibration among the different cage diastereomers in order to maximize the binding affinity of the system. Density functional theory was employed to rationalize the experimentally observed energy differences for C_{60} binding within the cage diastereomers. In contrast, the cage isomer based on a 2,7-pyrene scaffold has a more porous cavity and did not show affinity for neutral hydrophobic guests.

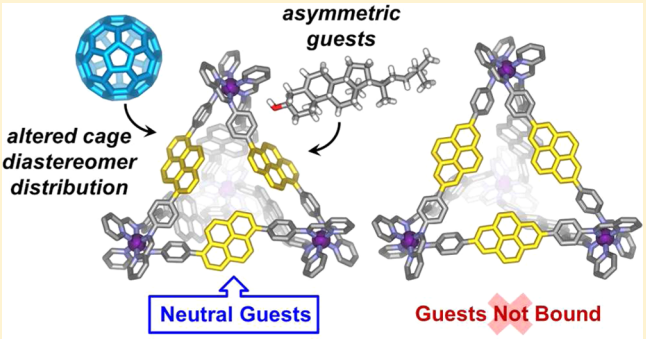

INTRODUCTION

Metal−organic cages[1] have attracted significant recent attention due to their wide-ranging applications[2] as photoreactors[3] and in gas sequestration,[4] catalysis,[5] stabilization of reactive species,[6] and generation of unusual reaction products.[7] These abiological structures are also of relevance as functional mimics of biological molecules such as protein receptors and enzymes. In order to extend the range of applications of synthetic metal−organic capsules toward the level of complexity exhibited by biological hosts it is necessary to create synthetic capsules capable of tightly and selectively binding large substrates. Cages assembled from ligands with extended aromatic panels[8] have shown promise as hosts for a variety of large neutral molecules.[9] Such hosts provide well-enclosed cavities isolated from their surroundings in addition to cage walls rich in π-electron density to provide favorable interactions with targeted guests. In addition to binding spherical[10] or planar aromatic guests of high symmetry,[11] the design of hosts for asymmetric molecules is necessary for potential applications such as drug delivery[12] and asymmetric catalysis.[13] The design of specifically tailored asymmetric hosts remains challenging[14] so it is desirable to employ hosts that can be readily prepared from simple symmetric building blocks.

Subcomponent self-assembly has been shown to be a versatile approach for the creation of increasingly complex architectures[15] which are obtained from simple building blocks through the formation of dynamic-covalent (C═N)[16] and coordinative (N → M) bonds during the same self-assembly process. We[15a,17] and others[18] have recently employed this technique to achieve a variety of functional ends, including to obtain tetrahedral structures with different shapes and varied molecular recognition properties, based on the self-assembly of iron(II) with amine-containing subcomponents and 2-formylpyridine.[9c,19] An inherent advantage of this approach is that the properties of the metal−organic cages can be readily altered[20] through variation of the subcomponents employed.[21] Herein we describe the preparation of two new Fe_4L_6 cages from two isomeric pyrene-containing diamines. The two cages display contrasting guest-binding properties depending on the arrangement of the pyrene panels around the surface of the cage; the cage based on a 1,6-pyrene scaffold provides a suitably isolated microenvironment for effective guest-binding while the 2,7-pyrene edged cage does not encapsulate neutral guests. In addition to examining the host−guest properties of the constitutionally isomeric cages, we show how different diastereomers of one of the cages contribute differentially to guest binding, which led to guest-induced adaptation on a system-wide level.

RESULTS AND DISCUSSION

Self-Assembly of Cages 1−2. Pyrene-containing subcomponents **A** and **B** were each synthesized in a single step from commercially available starting materials via Pd-catalyzed

Received: July 25, 2014
Published: October 14, 2014

   dx.doi.org/10.1021/ja507617h | J. Am. Chem. Soc. 2014, 136, 15615−15624

Scheme 1. Preparation of $[Fe_4L_6]^{8+}$ Tetrahedra 1 and 2 via Subcomponent Self-Assembly

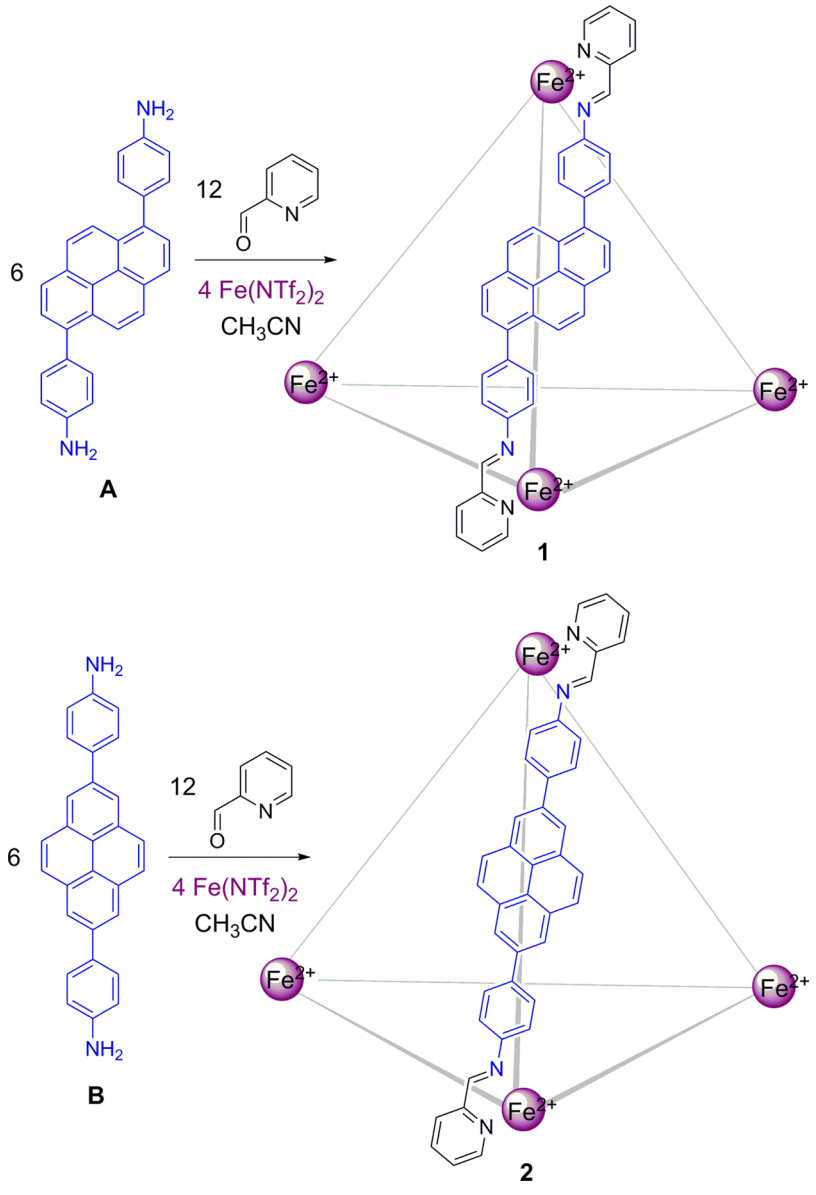

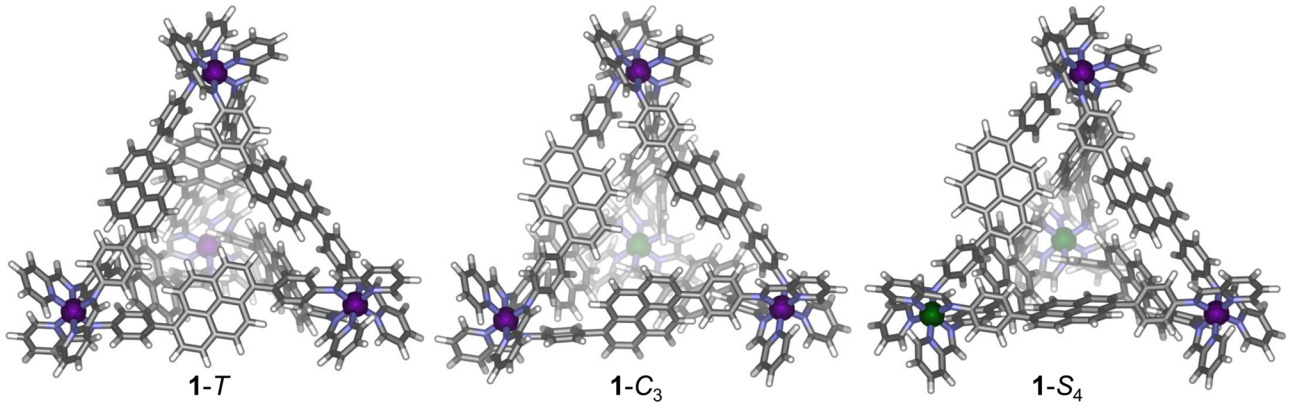

Figure 1. DFT-optimized structures of the three diastereomers of **1**. Fe^{II} centers with Δ and Λ stereochemistry are colored purple and green, respectively.

Suzuki–Miyaura cross-coupling reactions;[22] a full description of their synthesis is provided in the Supporting Information. The reaction of diamine **A** (6 equiv) with 2-formylpyridine (12 equiv) and iron(II) triflimide (4 equiv) yielded tetrahedral cage **1** (Scheme 1). The Fe_4L_6 stoichiometry of the assembly was

dx.doi.org/10.1021/ja507617h | J. Am. Chem. Soc. 2014, 136, 15615–15624

confirmed by electrospray ionization mass spectrometry (ESI-MS) (Supporting Information Figure S12).

Both the ^{1}H (Supporting Information Figure S5) and ^{13}C (Supporting Information Figure S7) NMR spectra of **1** were complicated; NMR signals were observed as clusters of peaks, consistent with a mixture of homochiral *T* (ΔΔΔΔ/ΛΛΛΛ),[23] heterochiral C_3 (ΔΔΔΛ/ΛΛΛΔ), and achiral S_4 (ΔΔΛΛ)[24] diastereomers[25] in equilibrium, as has been observed for other cages prepared via subcomponent self-assembly.[26] The DOSY (diffusion-ordered spectroscopy) spectrum of **1** confirmed that all peaks between 5.7 and 9.2 ppm had the same diffusion coefficient (Supporting Information Figure S11). Deconvolution of the imine region of the ^{1}H NMR spectrum of **1** gave percentages of 13%, 42%, and 45% for **1**-*T*, **1**-C_3, and **1**-S_4, respectively, which is close to the expected statistical distribution of 12.5% *T*, 50% C_3, and 37.5% S_4, suggesting that the three diastereomers are of similar energy. All efforts to grow X-ray quality single crystals of **1** were unsuccessful, likely due to the presence of diastereomers and possible further conformational complexity arising from different conformations of the offset pyrene groups.

Density functional theory (DFT) was employed in order to gain further insight into the structure of **1**. The structures of the three diastereomers of **1** (Figure 1) were optimized in the TURBOMOLE software package[27] using the PBE-D3 functional[28] and MIDI![29] (C, H, and N) and def2-TZVP[30] (Fe) basis sets. The three isomers are predicted to be similar in energy with a slight preference for **1**-S_4, which is predicted to be 11.7 and 18.0 kJ mol^{-1} more stable than **1**-C_3 and **1**-*T*, respectively, consistent with the observed distribution of diastereomers in solution. This observed diastereomer distribution indicates that they are nearly isoenergetic, placing the error in the DFT energies at ∼8 kJ mol^{-1}, which we consider reasonable, particularly given the difficulty in estimating differential rotational and vibrational contributions to entropy for systems of this size.

The metal−metal separations in **1** are calculated to be in the range 18.9−19.8 Å. The pyrene units in the energy-minimized structures display a variety of conformations. The cavity volume accessible for guest binding is expected to be strongly dependent on the conformation adopted by these groups in solution. The volume is expected to be maximized when the pyrene units adopt a conformation tangential to the edges of the tetrahedron as observed for four pyrene units in the DFT structures of **1**-*T* and **1**-C_3 but for only two pyrene units in **1**-S_4 (Figure 1). A tangential conformation of the pyrene units is also expected to maximize the degree of cavity enclosure and minimize the size of the pores through which solvent and guest species may diffuse, factors expected to lead to efficient guest encapsulation.[9a,b]

The reaction of diamine **B** (6 equiv) with 2-formylpyridine (12 equiv) and iron(II) triflimide (4 equiv) yielded tetrahedral cage **2** (Scheme 1) as the only observed product as indicated by NMR spectroscopy, ESI-MS, and elemental analysis. The ^{1}H NMR spectrum of **2** (Supporting Information Figure S14) revealed a mixture of three diastereomers, with the ratio of **2**-*T*:**2**-C_3:**2**-S_4 estimated to be 12%:45%:43%, which is close to the expected statistical distribution, as observed for cage **1**.

Vapor diffusion of benzene into an acetonitrile solution (1 mM) of **2**·$(NTf_2)_8$ containing $[^{n}Bu_4N]PF_6$ (10 equiv) gave crystals of **2**·$(PF_6)_8$ suitable for single-crystal X-ray diffraction analysis. Two representations of the X-ray structure of **2** are shown in Figure 2. Cage **2** crystallized in the triclinic space group $P\bar{1}$ with one complete cage molecule in the asymmetric unit. The crystals were found to contain the diastereomer of C_3 point symmetry, with both ΛΛΛΔ and ΔΔΔΛ enantiomers present in the unit cell, related by inversion symmetry. Of the six ligands that bridge the four octahedral iron(II) centers, three ligands display a *syn* conformation, bridging iron(II) centers of opposing handedness, and three adopt an *anti* conformation, linking iron(II) centers of the same handedness. The pyrene units of the *anti* ligands almost completely close the cage face that they define (Figure 2, top). The remaining three faces are more open, with large pores (Figure 2, bottom). The interior of **2** is filled with three partial-occupancy benzene molecules in the solid state. The metal−metal separations are in the ranges 20.4−20.7 Å and 20.8−20.9 Å for the *syn* and *anti* ligands respectively, placing this cage among the largest M_4L_6 species to be structurally characterized to date.[26a,31] In the solid state pairs of cage molecules associate through aromatic stacking interactions involving the most planar cage faces (Supporting Information Figure S75); these favorable intermolecular interactions coupled

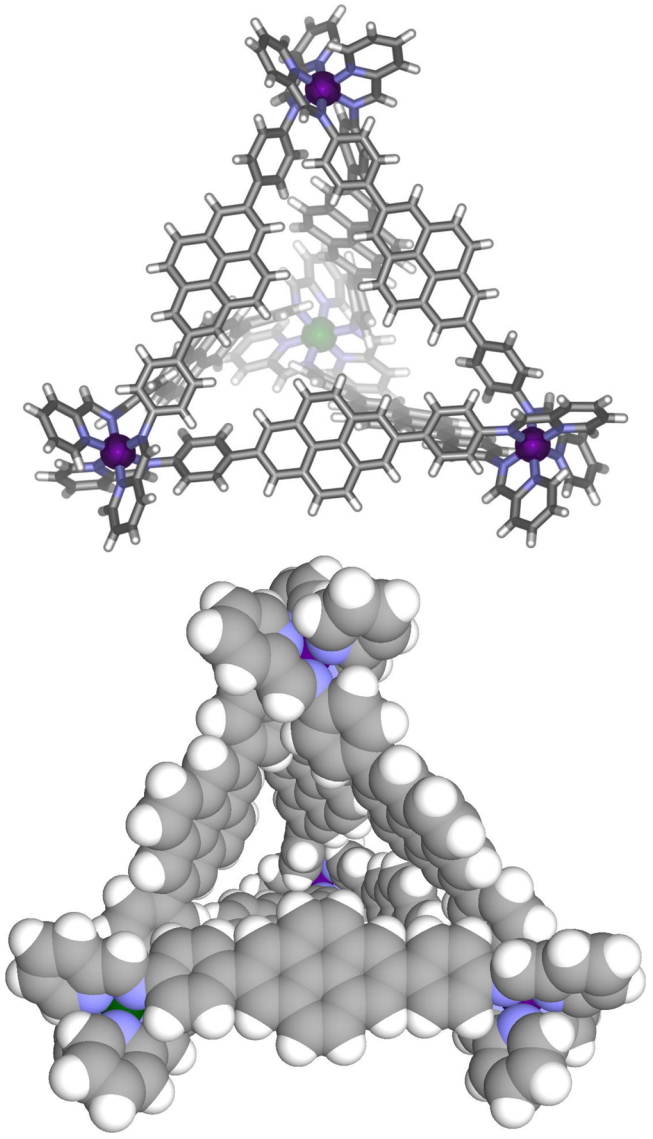

Figure 2. Two views of the cationic part of the crystal structure of **2**-C_3 showing the ΔΔΔΛ enantiomer: view down the pseudo-C_3-axis (top) and space-filling representation of the structure illustrating one of the open faces (bottom). Counterions, solvents, and disorder are omitted for clarity. Δ and Λ Fe^{II} centers are colored purple and green, respectively.

dx.doi.org/10.1021/ja507617h | J. Am. Chem. Soc. 2014, 136, 15615−15624

with the high abundance of the C_3 diastereomer in solution may explain the preferential crystallization[26] of this cage isomer.

Host–Guest Chemistry of Cage 1. To investigate the scope of guest binding within **1**, the molecules listed in Figure 3

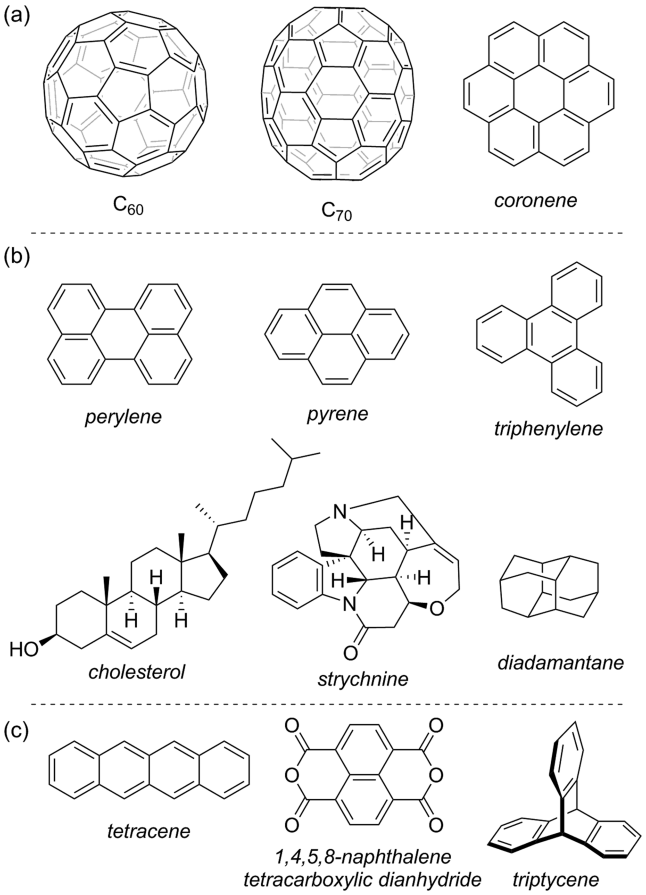

Figure 3. Prospective guest molecules for host **1**: (a) larger guests that show slow-exchange binding by NMR; (b) guests for which fast-exchange binding was observed; (c) compounds for which no evidence of encapsulation was observed.

were screened as potential guests. Each prospective guest (5 equiv) was added to a CD_3CN solution of host **1** (1–3 mM), and the mixture was allowed to equilibrate prior to the acquisition of NMR and mass spectra. UV–vis spectra were observed to undergo only minimal changes upon guest binding, and the fluorescence of the pyrene moieties was largely quenched by the Fe^{II} centers in the cages; hence, these techniques were not used to investigate guest binding. The addition of different guests brought about a re-equilibration among the different diastereomers of **1**, as the system adapted in order to maximize binding affinity.[26b]

Cage **1** was initially investigated as a fullerene receptor, because fullerenes were expected to interact with the pyrene moieties through $\pi-\pi$ stacking and have previously been shown to be encapsulated by metal–organic cages containing large aromatic panels.[9a−c,10,32] Both C_{60} and C_{70} were observed to form 1:1 host–guest complexes with cage **1** in CD_3CN. In each case host occupation was inferred through disappearance of the peaks corresponding to the free host and concurrent appearance of a new set of cage peaks corresponding to the host–guest complex. ESI-MS of the host–guest complexes confirmed formation of the 1:1 complexes $[C_{60} \subset \mathbf{1}]$ and $[C_{70} \subset \mathbf{1}]$; in each case the free host was no longer observed in the ESI mass spectrum (Supporting Information Figures S35 and S45).

The imine region of the ^{1}H NMR spectrum of $[C_{60} \subset \mathbf{1}]$ appeared simpler than that of cage **1**, displaying five signals of equal intensity, which corresponds to a 20%:80% mixture of the T and C_3 isomers (Figure 4). As these two isomers were equally amplified relative to the statistical distribution, we infer their C_{60} affinities to be similar. ^{1}H NMR spectra revealed no detectable amount of the S_4 isomer, suggesting that C_{60} binding in this isomer is not favorable. Examination of the phenyl resonances of $[C_{60} \subset \mathbf{1}]$ also revealed the presence of five magnetically distinct ligand environments: one for the T isomer and four for the C_3 isomer, (Figure 4 and Supporting Information Figure S28). For each of these environments, two distinct sets of signals attributable to those phenyl protons that are *endo* (H^6 and H^7) and those that are *exo* ($H^{6'}$ and $H^{7'}$) to the edge of the cage were observed, consistent with slow rotation of the phenyl rings on the NMR time scale, compared to the fast rotation observed for cage **1** in the absence of guest molecules. The phenyl resonances are also more dispersed relative to those of the empty cage due to contacts with the aromatic guest. Although C_{60} is effectively insoluble in CD_3CN,[34] the ^{13}C NMR spectrum of $[C_{60} \subset \mathbf{1}]$ in CD_3CN showed an intense resonance at 140.1 ppm, providing further confirmation of encapsulation of C_{60} by host **1** (Supporting Information Figure S29).

The binding energies of the three diastereomers of **1** with C_{60} were further probed through DFT calculations. The structures of $[C_{60} \subset \mathbf{1}\text{-}T]$, $[C_{60} \subset \mathbf{1}\text{-}C_3]$, and $[C_{60} \subset \mathbf{1}\text{-}S_4]$ were computed. The energy-minimized structures of $[C_{60} \subset \mathbf{1}]$ predicted all six pyrene units to lie tangentially to the edges of the cage, resulting in favorable $\pi-\pi$ interactions with the encapsulated C_{60} and a well-enclosed cavity. Pyrene units on opposite edges of the tetrahedron are separated by ca. 13 Å, and the cavity volumes of all three isomers are estimated to be in the range 625 ± 5 Å^3 using VOIDOO.[35] This void matches the size and shape of the spherical guest well (Figure 5).

The computed energies of binding (Table 1) match the experimentally observed trend. While the **1**-S_4 diastereomer is predicted to be thermodynamically favored when empty, the energetic cost of deforming it to accommodate the guest is significantly higher than predicted for the other two cage diastereomers, thereby disfavoring the formation of the $[C_{60} \subset \mathbf{1}\text{-}S_4]$ adduct. Examination of the overlaid empty and deformed structures (Supporting Information Figures S76–S78) shows that while only two pyrene rings must rotate to incorporate C_{60} in the C_3 and T diastereomers, four must rotate in the S_4 isomer. Even in the absence of accounting for the energy required to deform the cage (and guest) for binding, the host–guest complexation energy for **1**-S_4 is still the lowest out of the three isomers, consistent with the observation that C_{60} is not observed to bind to this diastereomer. Nevertheless, the span of binding energies of C_{60} to preorganized hosts is only 18.8 kJ/mol (line 4, Table 1), while the span of deformation energies required to organize the host diastereomers from their minimum-energy geometries is 51.9 kJ/mol; i.e., it is the deformation energy that is decisive for the change in diasteromeric population of the $C_{60} \subset \mathbf{1}$ isomers. The DFT analysis thus provides insight into both adaptation on the molecular level, through rotation of the pyrene units to provide a tailored guest-binding pocket, as well as the system-wide level through diastereomer interconversion,[26b] in order to express the diastereomers that form the most stable host–guest complexes.

dx.doi.org/10.1021/ja507617h | J. Am. Chem. Soc. 2014, 136, 15615–15624

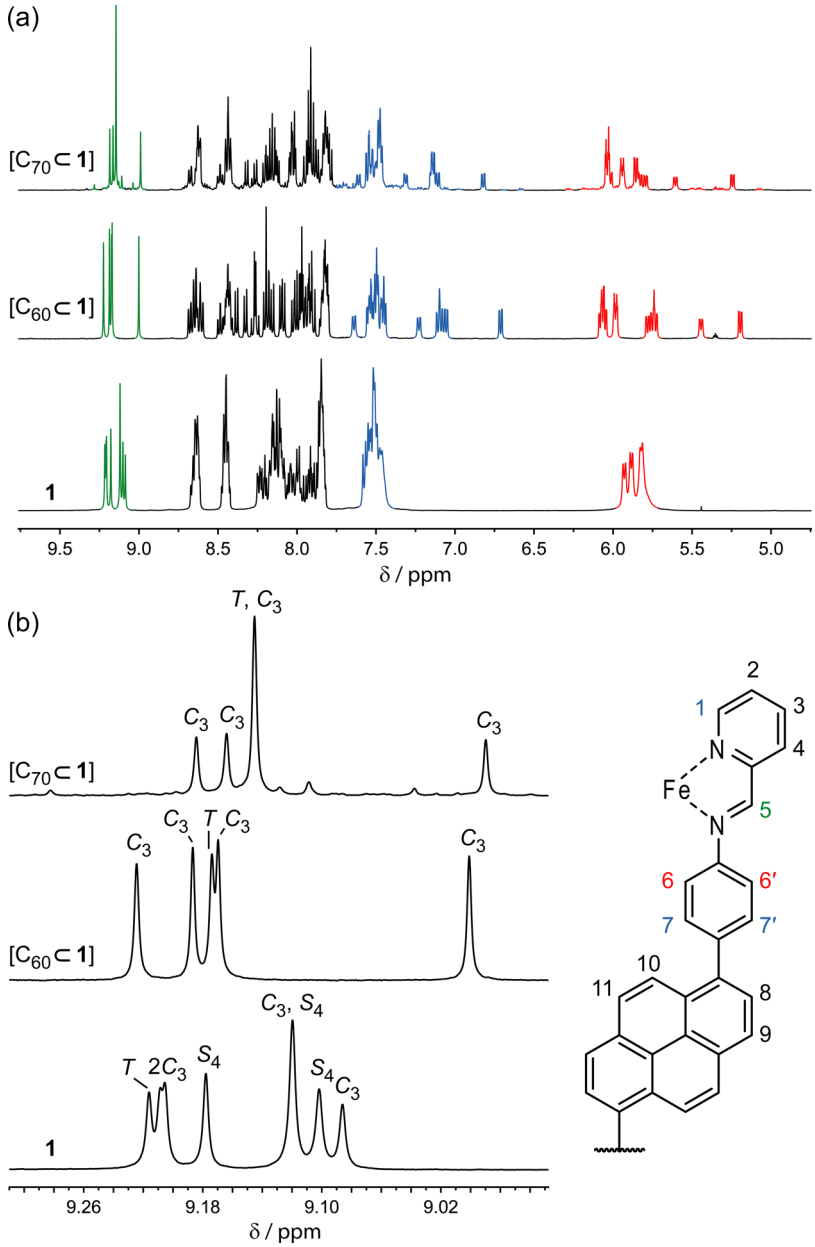

Figure 4. (a) Aromatic region of the ^{1}H NMR spectra (500 Hz, CD_3CN, 298 K) of cage **1**, [C_{60} ⊂ **1**] and [C_{70} ⊂ **1**]. The imine protons (H^5) are colored green, phenyl H^6 and $H^{6'}$ are colored red, and phenyl H^7, $H^{7'}$ and pyridyl H^1 are colored blue. (b) Expansion of the imine region of the ^{1}H NMR spectra of cage **1**, [C_{60} ⊂ **1**] and [C_{70} ⊂ **1**] with the peaks for the *T*, C_3, and S_4 isomers labeled.[33]

Similar trends were observed in the ^{1}H NMR spectrum of [C_{70} ⊂ **1**]; the distribution of the *T*, C_3, and S_4 isomers was estimated to be 32%, 63%, and 5%. As observed for [C_{60} ⊂ 1], the C_3 isomer was the most abundant species in the host–guest mixture while the S_4 isomer was disfavored compared to the ratio observed for the free host **1** (Figure 4). However, the *T* isomer shows the largest amplification relative to the statistical distribution, suggesting that it formed the most stable host–guest complex with the larger C_{70} guest.

Host **1** could be utilized for the extraction of fullerenes from fullerene soot. When **1** (5% by weight) was agitated with fullerene soot in CH_3CN for 10 days at 343 K, the ESI-MS showed peaks corresponding to [C_{60} ⊂ **1**] and [C_{70} ⊂ **1**] with intensities in a ratio of roughly 1:1 (Supporting Information Figure S47), compared to the reported abundances of 66.6% and 23.4% for C_{60} and C_{70}, respectively, in the commercial product.[36] This observation suggests that **1** has a slight preference for encapsulation of C_{70} over C_{60}. Traces of host–guest complexes of higher fullerenes were also detected.

No guest substitution was detected by ^{1}H NMR or ESI-MS when excess C_{70} was added to a solution of [C_{60} ⊂ **1**] following 7 days at 343 K (Supporting Information Figures S48 and S49), nor when excess C_{60} was added to a solution of [C_{70} ⊂ **1**] (Supporting Information Figure S50 and S51). We infer that guest release rates for C_{60} and C_{70} are slow, resulting in the fullerene guests becoming kinetically trapped inside the cavity of **1** under the experimental conditions employed.[37]

Further binding studies of large hydrophobic guest molecules were carried out using planar polycyclic aromatic hydrocarbons (PAHs). The addition of excess coronene (5 equiv) to **1** in CD_3CN resulted in broadening of the ^{1}H NMR spectrum to such a degree that peaks for individual cage diastereomers could no

dx.doi.org/10.1021/ja507617h | *J. Am. Chem. Soc.* 2014, 136, 15615–15624

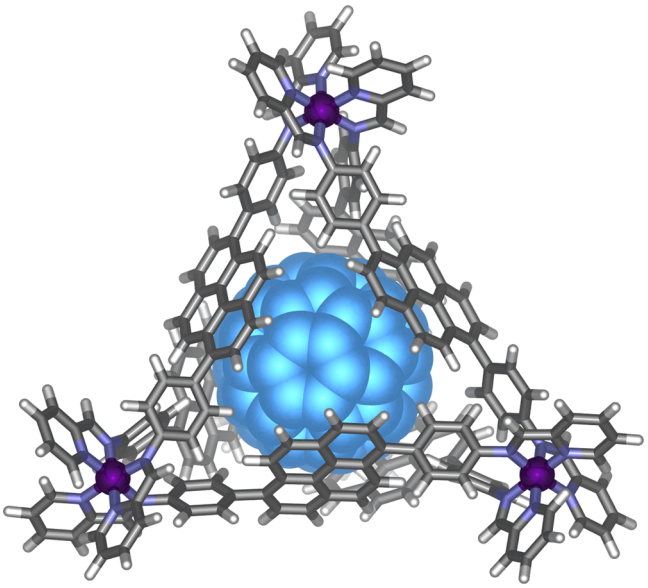

Figure 5. DFT-optimized structure of $[C_{60} \subset \mathbf{1}]$. The ΔΔΔΛ enantiomer of the most abundant C_3 isomer is shown with the Λ Fe^{II} center behind the fullerene.

Table 1. DFT Electronic Energies in kJ/mol for Each Diastereomer of 1 and $[C_{60} \subset \mathbf{1}]$ Relative to 1-C_3 and $[C_{60} \subset$ 1-$C_3]$, Respectively

E (kJ mol^{-1})	1-C_3	1-S_4	1-T
1 $E_{relative}$	0.0	−11.7	6.3
$[C_{60} \subset \mathbf{1}]$ $E_{relative}$	0.0	59.4	22.2
$\Delta E_{deformation}$ [a]	33.9	85.8	41.0
$\Delta E_{host-guest} - \Delta E_{deformation}$ [b]	−515.9	−497.1	−507.5

[a]Energy of host at geometry adopted in complex relative to relaxed geometry when empty. [b]Energy of guest binding with host predistorted to geometry found in complex.

longer be resolved (Supporting Information Figure S52). ESI-MS of the mixture suggested formation of a host−guest complex in which exactly 2 equiv of coronene were encapsulated per host (Supporting Information Figure S55). The encapsulated coronene gave rise to a broad ^{1}H NMR signal at 5.66 ppm, which is shifted significantly upfield relative to that of free coronene at 9.03 ppm. The broad NMR of $[\text{coronene}_2 \subset \mathbf{1}]$ could be due to an intermediate rate of exchange between free and bound guests on the NMR time scale, or to tumbling of the bound coronenes within host **1**. Cooling a CD_3CN solution of $[\text{coronene}_2 \subset \mathbf{1}]$ to 233 K led to a sharpening and increase in number of signals in the ^{1}H NMR spectrum (Supporting Information Figure S54), although dynamic behavior was not completely frozen out within the temperature range accessible in CD_3CN. The DOSY spectrum of $[\text{coronene}_2 \subset \mathbf{1}]$ at 233 K (Supporting Information Figure S53) confirmed that the signals of coronene diffused at the same rate as those of the host, supporting guest encapsulation.

The addition of excess C_{60} (5 equiv) to a CD_3CN solution of $[\text{coronene}_2 \subset \mathbf{1}]$ resulted in complete displacement of the coronene in favor of C_{60}: $[C_{60} \subset \mathbf{1}]$ was the only product observed by ^{1}H NMR and ESI-MS following 12 h at 323 K. Therefore, we infer that C_{60} binds more strongly within **1** compared to coronene, possibly due to a better size and shape match between the host cavity and the spherical guest, resulting in maximization of favorable π−π interactions. Of course, there is also an entropic preference for a 1:1 host−guest complex versus a 1:2 alternative.

The addition of any of the smaller PAHs perylene, pyrene, or triphenylene (Figure 3) to **1** resulted in host occupation by a guest that was observed to exchange rapidly between free and bound states on the NMR time scale. This behavior was signaled by small shifts to the ^{1}H NMR resonances of **1** and broadening of some host peaks, along with upfield shifts in the guest signals (Supporting Information Figures S57−S59). ESI mass spectra of the host−guest mixtures displayed multiple $(\text{guest})_n \subset \mathbf{1}$ (n = 0−4) adducts. These guests are inferred to be too small to bind tightly within the cavity of **1**. Fast-exchange binding was also observed for aliphatic diadamantane (Supporting Information Figure S60) while no evidence of interaction was observed between **1** and triptycene, tetracene, or 1,4,5,8-naphthalene tetracarboxylic dianhydride.

We also investigated cage **1** as a host for asymmetric natural-product molecules and derivatives. Steroid derivatives were chosen for initial studies due to their importance in biological systems and as therapeutic agents, as well as their known ability to form complexes with aromatic substrates in the solid state.[38] The addition of cholesterol (1 equiv) to a solution of host **1** in CD_3CN (1 mM) gave a single set of cholesterol resonances, shifted upfield by up to 1.1 ppm relative to those of free cholesterol (Figure 6a). This observation is consistent with host−guest complexation in fast exchange on the NMR time scale. The host signals were also broadened, and additional peaks were observed in the imine region, consistent with desymmeterization as a result of interaction with the asymmetric guest. The ^{1}H DOSY NMR spectrum of the mixture confirmed that all aromatic signals belong to cage **1**. The diffusion coefficients of the cholesterol resonances were reduced relative to those of the unbound guest, consistent with binding to host **1** under fast exchange on the NMR time scale (Supporting Information Figure S63). The addition of excess C_{60} (5 equiv) to the mixture of **1** and cholesterol resulted in complete conversion to $[C_{60} \subset \mathbf{1}]$, with the cholesterol resonances returning to chemical shifts characteristic of the free guest, providing further evidence for binding of cholesterol within the cavity of **1** (Supporting Information Figure S62) rather than through interaction with the exterior of the cage. A Job plot (Supporting Information Figure S64) suggested that a 1:1 binding stoichiometry dominates at 1 mM concentration.

Upon titration of cholesterol into a solution of **1**, its imine signals were observed to disperse and shift downfield, with different signals showing variable degrees of response to the presence of the guest (Figure 6b). Three signals were sufficiently sharp and separated from the others for their chemical shifts to be monitored and fit to 1:1 binding isotherms, giving association constants of $1.0 \pm 0.2 \times 10^3$ M^{-1} and $1.6 \pm 0.5 \times 10^3$ M^{-1} from peaks tentatively assigned to the C_3 isomer and $5 \pm 1 \times 10^3$ M^{-1} from the peak for the T isomer (Supporting Information Figures S67−S69). As with fullerenes, these results are consistent with the different diastereomers of **1** contributing differentially to the binding of cholesterol. The errors in the calculated association constants, however, preclude certainty.

The steroidal hormones progesterone and testosterone as well as the synthetic derivative fludrocortisone also bound within **1**, as inferred from clear shifts in the ^{1}H NMR spectra of the guests (Supporting Information Figures S70−S72) in the presence of **1**, indicating that this cage shows promise as a host for a variety of steroids. In each case the chemical shift changes were more modest than those observed for cholesterol, suggesting that **1** is a

dx.doi.org/10.1021/ja507617h | J. Am. Chem. Soc. 2014, 136, 15615−15624

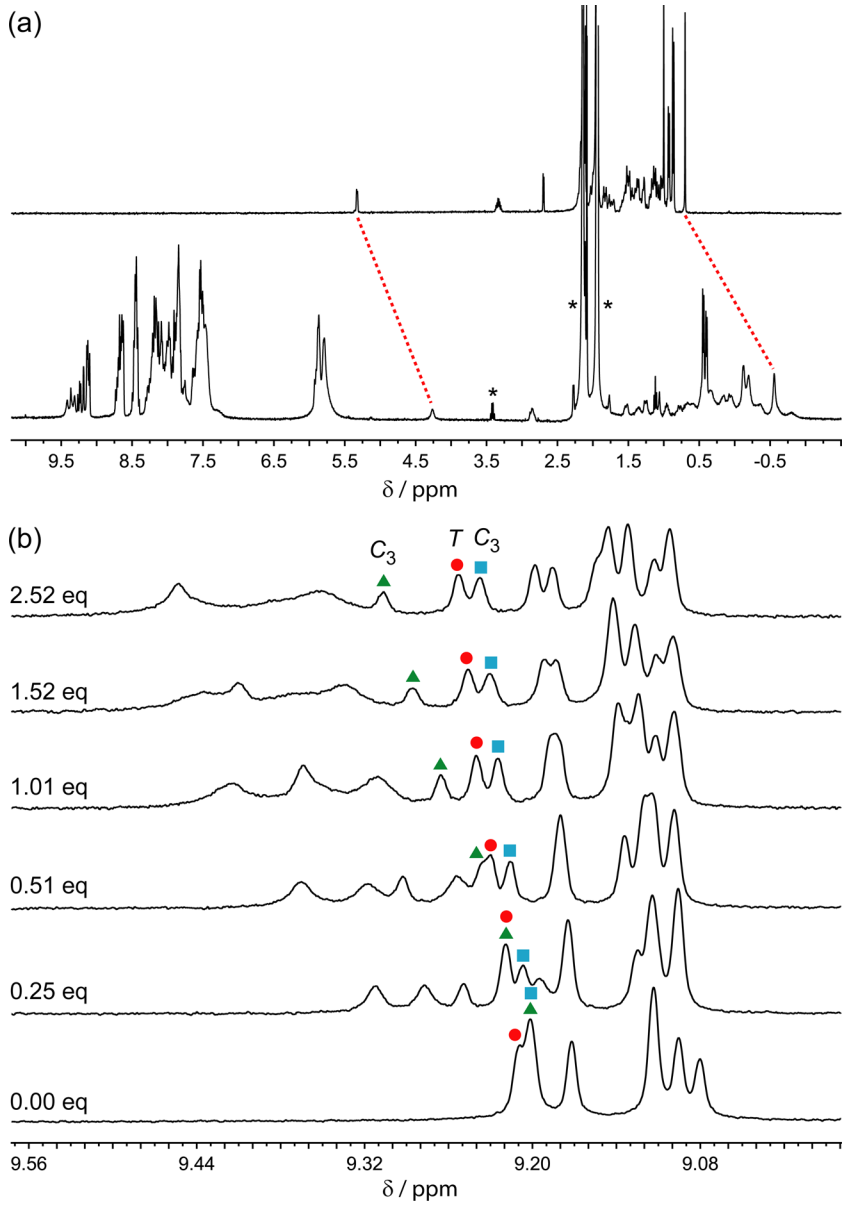

Figure 6. (a) Bottom: ^{1}H NMR spectrum (400 MHz, 298 K, CD_3CN) of a mixture of **1** (1 mM) and cholesterol (1 mM). Top: ^{1}H NMR spectrum (400 MHz, 298 K, CD_3CN) of cholesterol (1 mM). Shifts in selected cholesterol signals are marked with red dashed lines, and solvent peaks are marked by an asterisk. (b) Expansion of the imine region of the ^{1}H NMR spectrum (400 MHz, 298 K, CD_3CN) of **1** following the progressive addition of 0−2.52 equiv of cholesterol. Chemical shifts that were fit to 1:1 binding isotherms are marked with green triangles, red circles, and blue squares.

weaker host for these more polar steroids. Intriguingly, no evidence of interaction was observed with androsterone and estradiol, despite the chemical similarity of these steroids to those observed to bind within **1**.

Fast-exchange guest binding was also observed for the alkaloid strychnine, although ^{1}H NMR chemical shift changes upon guest binding were less pronounced for this smaller guest (Supporting Information Figure S73).

Host−Guest Chemistry of Cage 2. Cage **2** was investigated as a host for each hydrophobic guest that was observed to bind within **1** (Figure 3). However, in all cases no encapsulation was inferred to have taken place, as the ^{1}H NMR signals for **2** appeared at the same chemical shifts as in the absence of the guest and the signals for all acetonitrile soluble guests were identical or very close[39] to those in the absence of host. We infer the marked reduction in guest binding ability of cage **2** compared to **1** to be due to the cavity of **2** not being sufficiently enclosed to constrain potential guests inside.

CONCLUSIONS

In conclusion we have shown that two isomeric pyrene-edged cages show very different host−guest properties depending on the arrangement of the pyrene groups around the surface of the tetrahedron. Cage **2**, based on a 2,7-pyrene scaffold with an open cavity, was not observed to bind neutral guests. In contrast, isomeric cage **1**, based on a 1,6-pyrene scaffold, is able to provide a well-enclosed cavity and is a good host for large aromatic and hydrophobic guests, demonstrating the importance of cavity enclosure for strong host−guest interactions. This cage was shown to adapt when binding fullerenes, amplifying the diastereomers best able to bind the guest in order to maximize binding affinity. DFT analysis provided insights into the origin of

dx.doi.org/10.1021/ja507617h | J. Am. Chem. Soc. 2014, 136, 15615−15624

this adaptive response, which is primarily driven by differential distortion energies required to transform free host geometries to those geometries required to encapsulate guests. In addition to binding symmetric guests, cage **1** also displayed binding affinity for steroid derivatives, allowing these asymmetric guests to be bound without the need to design an asymmetric host. Future work will investigate whether the reactivity of these guests can be altered through encapsulation.

EXPERIMENTAL METHODS

General. Unless otherwise specified, all starting materials were purchased from commercial sources and used as supplied. NMR spectra were recorded on a Bruker DRX-400, Bruker Avance 500 Cryo, and a Bruker 500 TCI-ATM Cryo. ^{1}H chemical shifts (δ) are reported in parts per million (ppm) and are reported relative to the solvent residual peaks. ^{19}F chemical shifts (δ) are reported relative to hexafluorobenzene at −164.9 ppm. Low-resolution electrospray ionization mass spectra (ESI-MS) were obtained on a Micromass Quattro LC and high-resolution mass spectra acquired using a Thermofisher LTQ Orbitrap XL.

Synthesis of Cage ***1****.* Iron(II) triflimide (138 mg, 0.195 mmol), 1,6-bis(4-aminophenyl)pyrene (**A**, 113 mg, 0.294 mmol), and 2-formylpyridine (56 μL, 0.59 mmol) were dissolved in acetonitrile (100 mL). The reaction mixture was stirred under nitrogen at room temperature for 24 h. The volume was reduced to 50 mL *in vacuo*. The solution was layered with diethyl ether (100 mL) and kept at −4 °C for 24 h. The deep purple microcrystalline solid was filtered and washed with excess diethyl ether. Yield 221 mg, 95%. ^{1}H NMR (500 MHz; 298 K; CD_3CN): δ 9.21−9.06 (12H, imine), 8.68−8.61 (12H, pyridyl), 8.48−8.42 (12H, pyridyl), 8.26−7.81 (60H, pyrene, pyridyl), 7.60−7.43 (36H, phenyl, pyridyl), 5.96−5.77 (24H, phenyl). ^{13}C NMR (126 MHz, 298 K, CD_3CN): δ 176.2−175.8 (imine), 159.3, 157.0, 156.9, 151.0−150.5, 142.6−142.3, 140.8, 137.4−137.2, 132.4, 131.6−131.3, 131.1−130.8, 129.4−128.5, 126.2−125.3, 124.7, 122.9−122.4, 122.1, 119.6. ^{19}F NMR (376 MHz; 298 K; CD_3CN): δ −80.5 (s, NTf_2^-). ESI-MS: m/z = 449.9 $[\mathbf{1}]^{8+}$, 554.2 $[\mathbf{1}(NTf_2^-)]^{7+}$, 693.3 $[\mathbf{1}(NTf_2^-)_2]^{6+}$, 887.8 $[\mathbf{1}(NTf_2^-)_3]^{5+}$, 1179.9 $[\mathbf{1}(NTf_2^-)_4]^{4+}$. Anal. (%) Calcd for $C_{256}H_{156}F_{48}Fe_4N_{32}O_{32}S_{16}\cdot 2H_2O$: C, 52.31%; H, 2.75%; N, 7.63%. Found: C, 52.15%; H, 2.74%; N, 7.70%.

Synthesis of Cage ***2****.* Iron(II) triflimide (132 mg, 0.187 mmol), 2,7-bis(4-aminophenyl)pyrene (**B**, 108 mg, 0.281 mmol), and 2-formylpyridine (53 μL, 0.56 mmol) were dissolved in acetonitrile (100 mL). The reaction mixture was stirred under nitrogen at room temperature for 24 h. The volume was reduced to 50 mL *in vacuo*. The solution was layered with diethyl ether (100 mL) and kept at −4 °C for 24 h. The deep purple microcrystalline solid was filtered and washed with excess diethyl ether. Yield 201 mg, 74%. ^{1}H NMR (500 MHz; 298 K; CD_3CN): δ 9.09−8.91 (12H, imine), 8.73−8.67 (12H, pyrene), 8.64−8.56 (24H, pyrene, pyridyl), 8.48−8.43 (12H, pyridyl), 8.36−8.31 (12H, pyrene), 8.29−8.26 (12H, pyrene), 8.04−7.96 (12H, phenyl), 7.93−7.79 (24H, phenyl, pyridyl), 7.56−7.43 (12H, pyridyl), 5.84−5.62 (24H, phenyl). ^{13}C NMR (126 MHz, 298 K, CD_3CN): δ 175.9−175.2 (imine), 159.3−158.9, 156.8−156.5, 151.0−150.3, 142.3−141.4, 140.8−140.4, 138.3−137.6, 132.8−132.4, 132.3−131.8, 131.1−130.5, 129.8−128.7, 125.5, 124.9−124.2, 123.4−122.7, 122.3, 119.1. ^{19}F NMR (376 MHz; 298 K; CD_3CN): δ −80.4 (s, NTf_2^-). ESI-MS: m/z = 449.9 $[\mathbf{2}]^{8+}$, 554.2 $[\mathbf{2}(NTf_2^-)]^{7+}$, 693.3 $[\mathbf{2}(NTf_2^-)_2]^{6+}$, 887.8 $[\mathbf{2}(NTf_2^-)_3]^{5+}$, 1179.9 $[\mathbf{2}(NTf_2^-)_4]^{4+}$. Anal. (%) Calcd for $C_{256}H_{156}F_{48}Fe_4N_{32}O_{32}S_{16}$: C, 52.64%; H, 2.69%; N, 7.67%. Found: C, 52.73%; H, 2.72%; N, 7.68%.

General Procedure for Host−Guest Investigations. A solution of **1** or **2** in CD_3CN (1.0−3.0 mM) was transferred to an NMR tube, and the prospective guest molecule (typically ∼5 equiv) was added as a solid. The mixture was sonicated for 10 min and allowed to equilibrate for at least 24 h at 298 K prior to measurement of the NMR and mass spectra. Characterization of the resulting host−guest complexes is given in the Supporting Information.

X-ray Crystallography. Crystals of $\mathbf{2}\cdot 8PF_6\cdot 2.5C_6H_6\cdot 0.5MeCN$ were grown by diffusion of benzene into an acetonitrile solution of $\mathbf{2}\cdot 8NTf_2$ containing 10 equiv of $[^nBu_4N]PF_6$. Data were collected at Beamline I19 of Diamond Light Source[40] employing silicon double crystal monochromated synchrotron radiation (0.6889 Å) with ω scans at 100(2) K.[41] Data were treated with ECLIPSE,[42] and integration and reduction were undertaken with SAINT and XPREP.[43] Subsequent computations were carried out using the WinGX-32 graphical user interface.[44] A multiscan empirical absorption correction was applied to the data using SADABS.[43] The structure was solved by direct methods using SUPERFLIP[45] and then refined and extended with SHELXL-2013.[46] In general, non-hydrogen atoms with occupancies greater than 0.5 were refined anisotropically. Carbon-bound hydrogen atoms were included in idealized positions and refined using a riding model. Disorder was modeled using standard crystallographic methods including constraints, restraints, and rigid bodies where necessary. The crystals employed rapidly lost solvent after removal from the mother liquor, and rapid handling prior to quenching in the cryostream was required to collect data. Despite these measures and the use of synchrotron radiation, few reflections at greater than 1.02 Å resolution were observed. One of the pyrene groups shows positional disorder and was modeled in two parts with isotropic thermal parameters. The eight PF_6^- anions were modeled as disordered over nine lattice sites, seven of which show additional positional disorder. The benzene solvent molecules also show substantial disorder and were modeled with rigid body constraints (AFIX 66). The SQUEEZE[47] function of PLATON[48] was employed to remove the contribution of the electron density associated with further disordered solvent molecules.

Crystallographic data are summarized here: formula $C_{256}H_{172.5}F_{48}Fe_4N_{24.5}P_8$, M_r 4974.83, triclinic, space group $P\bar{1}$ (No. 2), a 24.4345(15), b 25.6731(16), c 28.6611(17) Å, α 82.922(3)°, β 66.366(4)°, γ 72.449(3)°, V 15704.5(17) Å^3, D_c 1.052 g cm^{-3}, Z 2, crystal size 0.01 by 0.01 by 0.01 mm^3, color purple, habit block, temperature 100(2) K, λ(synchrotron) 0.6889 Å, μ(synchrotron) 0.296 mm^{-1}, T(SADABS)$_{min,max}$ 0.6133, 0.7445, $2\theta_{max}$ 39.47, *hkl* range −23 23, −25 25, −28 28, N 107 323, N_{ind} 30 894 (R_{merge} 0.0998), N_{obs} 18 375($I > 2\sigma(I)$), N_{var} 2834, residuals R1(F) 0.1016, wR2(F^2) 0.3111, GOF(all) 1.054, $\Delta\rho_{min,max}$ −0.725, 1.011 e$^-$ Å^{-3}.

Computational Methods. All calculations were performed using the PBE-D3 density functional[28] with Becke−Johnson damping[49] as implemented in the TURBOMOLE 6.4 software package. Initial structures for each of the diastereomers of **1** were arranged so that all of the pyrene moieties were approximately equivalently disposed, but over the course of optimization, some of the pyrenes in the empty C_3 and S_4 isomers rotated. As a result, the final structures for the C_3 and S_4 isomers and their host−guest complexes have ratios of 3:3 left-to-right flipped pyrene moieties.

The heteroatom-polarized split-valence MIDI! basis set[29] was used for H, C, and N atom types, and the def2-TZVP basis set[30] for Fe atoms. A resolution of the identity procedure was employed, using the def2-TZVP fitting basis implemented in TURBOMOLE[27] for Fe atoms and def-SVP[50] for H, C, and N atom types. The MIDI! and def-SVP fitting basis sets were employed to keep the calculations (particularly of the host−guest complexes) tractable.

One consequence of the large sizes of the various structures was that the standard convergence criteria for geometry optimization in TURBOMOLE[27] were generally found to be too strict to be practical. Consequently, more lenient convergence criteria were employed, namely, the energy was required to change by less than 0.4 kJ/mol cumulatively over the course of five consecutive geometry-optimization steps.

ASSOCIATED CONTENT

Supporting Information

Synthetic procedures and characterization of subcomponents **A** and **B**, characterization of complexes **1** and **2**, spectroscopic data, details of guest-binding investigations and characterization of host−guest complexes, and the CIF file for **2**. This material is available free of charge via the Internet at http://pubs.acs.org. Crystallographic data deposited with the Cambridge Crystallographic Data Centre as entry CCDC 1015565.

AUTHOR INFORMATION

Corresponding Author

jrn34@cam.ac.uk

Notes

The authors declare no competing financial interest.

ACKNOWLEDGMENTS

This work was supported by the UK Engineering and Physical Sciences Research Council (EPSRC) and the US National Science Foundation (NSF CHE-1124244). We thank the EPSRC Mass Spectrometry Service at Swansea for carrying out the high resolution mass spectrometry and Diamond Light Source (UK) for synchrotron beamtime on I19 (MT8464). We also thank Dr Salvatore Zarra, Derrick A. Roberts and the NMR service team at the Department of Chemistry, University of Cambridge for performing some NMR experiments and Professor David A. Vosburg for helpful discussions.

REFERENCES

(1) (a) Han, M.; Engelhard, D. M.; Clever, G. H. *Chem. Soc. Rev.* **2014**, *43*, 1848. (b) Harris, K.; Fujita, D.; Fujita, M. *Chem. Commun.* **2013**, *49*, 6703. (c) Ronson, T. K.; Fisher, J.; Harding, L. P.; Hardie, M. J. *Angew. Chem., Int. Ed.* **2007**, *46*, 9086. (d) Gütz, C.; Hovorka, R.; Klein, C.; Jiang, Q.-Q.; Bannwarth, C.; Engeser, M.; Schmuck, C.; Assenmacher, W.; Mader, W.; Topić, F.; Rissanen, K.; Grimme, S.; Lützen, A. *Angew. Chem., Int. Ed.* **2014**, *53*, 1693. (e) Ghosh, K.; Hu, J.; White, H. S.; Stang, P. J. *J. Am. Chem. Soc.* **2009**, *131*, 6695. (f) Custelcean, R.; Bonnesen, P. V.; Duncan, N. C.; Zhang, X.; Watson, L. A.; Van Berkel, G.; Parson, W. B.; Hay, B. P. *J. Am. Chem. Soc.* **2012**, *134*, 8525. (g) Mukherjee, S.; Mukherjee, P. S. *Chem. Commun.* **2014**, *50*, 2239.

(2) Ward, M. D.; Raithby, P. R. *Chem. Soc. Rev.* **2013**, *42*, 1619.

(3) (a) Yoshizawa, M.; Miyagi, S.; Kawano, M.; Ishiguro, K.; Fujita, M. *J. Am. Chem. Soc.* **2004**, *126*, 9172. (b) Yoshizawa, M.; Takeyama, Y.; Okano, T.; Fujita, M. *J. Am. Chem. Soc.* **2003**, *125*, 3243.

(4) Duriska, M. B.; Neville, S. M.; Lu, J.; Iremonger, S. S.; Boas, J. F.; Kepert, C. J.; Batten, S. R. *Angew. Chem., Int. Ed.* **2009**, *48*, 8919.

(5) (a) Yoshizawa, M.; Tamura, M.; Fujita, M. *Science* **2006**, *312*, 251. (b) Hastings, C. J.; Pluth, M. D.; Bergman, R. G.; Raymond, K. N. *J. Am. Chem. Soc.* **2010**, *132*, 6938. (c) Murase, T.; Horiuchi, S.; Fujita, M. *J. Am. Chem. Soc.* **2010**, *132*, 2866. (d) Kuil, M.; Soltner, T.; van Leeuwen, P.; Reek, J. N. H. *J. Am. Chem. Soc.* **2006**, *128*, 11344. (e) Jiao, Y.; Wang, J.; Wu, P.; Zhao, L.; He, C.; Zhang, J.; Duan, C. *Chem.—Eur. J.* **2014**, *20*, 2224. (f) Otte, M.; Kuijpers, P. F.; Troeppner, O.; Ivanović-Burmazović, I.; Reek, J. N. H.; de Bruin, B. *Chem.—Eur. J.* **2013**, *19*, 10170. (g) Samanta, D.; Mukherjee, S.; Patil, Y. P.; Mukherjee, P. S. *Chem.—Eur. J.* **2012**, *18*, 12322.

(6) (a) Nakabayashi, K.; Kawano, M.; Fujita, M. *Angew. Chem., Int. Ed.* **2005**, *44*, 5322. (b) Horiuchi, S.; Murase, T.; Fujita, M. *J. Am. Chem. Soc.* **2011**, *133*, 12445. (c) Yoshizawa, M.; Kusukawa, T.; Fujita, M.; Yamaguchi, K. *J. Am. Chem. Soc.* **2000**, *122*, 6311.

(7) Furusawa, T.; Kawano, M.; Fujita, M. *Angew. Chem., Int. Ed.* **2007**, *46*, 5717.

(8) (a) Johnson, D. W.; Raymond, K. N. *Inorg. Chem.* **2001**, *40*, 5157. (b) Tidmarsh, I. S.; Faust, T. B.; Adams, H.; Harding, L. P.; Russo, L.; Clegg, W.; Ward, M. D. *J. Am. Chem. Soc.* **2008**, *130*, 15167.

(9) (a) Kishi, N.; Li, Z.; Yoza, K.; Akita, M.; Yoshizawa, M. *J. Am. Chem. Soc.* **2011**, *133*, 11438. (b) Meng, W.; Breiner, B.; Rissanen, K.; Thoburn, J. D.; Clegg, J. K.; Nitschke, J. R. *Angew. Chem., Int. Ed.* **2011**, *50*, 3479. (c) Mahata, K.; Frischmann, P. D.; Würthner, F. *J. Am. Chem. Soc.* **2013**, *135*, 15656. (d) Mirtschin, S.; Slabon-Turski, A.; Scopelliti, R.; Velders, A. H.; Severin, K. *J. Am. Chem. Soc.* **2010**, *132*, 14004.

(10) Kishi, N.; Akita, M.; Kamiya, M.; Hayashi, S.; Hsu, H.-F.; Yoshizawa, M. *J. Am. Chem. Soc.* **2013**, *135*, 12976.

(11) (a) Li, K.; Zhang, L.-Y.; Yan, C.; Wei, S.-C.; Pan, M.; Zhang, L.; Su, C.-Y. *J. Am. Chem. Soc.* **2014**, *136*, 4456. (b) Zheng, Y.-R.; Zhao, Z.; Kim, H.; Wang, M.; Ghosh, K.; Pollock, J. B.; Chi, K.-W.; Stang, P. J. *Inorg. Chem.* **2010**, *49*, 10238.

(12) (a) Therrien, B. *Chem.—Eur. J.* **2013**, *19*, 8378. (b) Lewis, J. E. M.; Gavey, E. L.; Cameron, S. A.; Crowley, J. D. *Chem. Sci.* **2012**, *3*, 778.

(13) Lee, S. J.; Hu, A.; Lin, W. *J. Am. Chem. Soc.* **2002**, *124*, 12948.

(14) (a) Nakamura, T.; Ube, H.; Shionoya, M. *Chem. Lett.* **2013**, *42*, 328. (b) Meng, W.; Ronson, T. K.; Nitschke, J. R. *Proc. Natl. Acad. Sci. U.S.A.* **2013**, *110*, 10531. (c) Han, M.; Michel, R.; Clever, G. H. *Chem.—Eur. J.* **2014**, *20*, 10640.

(15) (a) Ronson, T. K.; Zarra, S.; Black, S. P.; Nitschke, J. R. *Chem. Commun.* **2013**, *49*, 2476. (b) Reichel, F.; Clegg, J. K.; Gloe, K.; Gloe, K.; Weigand, J. J.; Reynolds, J. K.; Li, C.-G.; Aldrich-Wright, J. R.; Kepert, C. J.; Lindoy, L. F.; Yao, H.-C.; Li, F. *Inorg. Chem.* **2014**, *53*, 688. (c) Sham, K.-C.; Yiu, S.-M.; Kwong, H.-L. *Inorg. Chem.* **2013**, *52*, 5648.

(16) Belowich, M. E.; Stoddart, J. F. *Chem. Soc. Rev.* **2012**, *41*, 2003.

(17) Castilla, A. M.; Ramsay, W. J.; Nitschke, J. R. *Acc. Chem. Res.* **2014**, *47*, 2063.

(18) (a) Campbell, V. E.; Guillot, R.; Riviere, E.; Brun, P.-T.; Wernsdorfer, W.; Mallah, T. *Inorg. Chem.* **2013**, *52*, 5194. (b) Bunzen, H.; Nonappa; Kalenius, E.; Hietala, S.; Kolehmainen, E. *Chem.—Eur. J.* **2013**, *19*, 12978. (c) Zhou, X.-P.; Wu, Y.; Li, D. *J. Am. Chem. Soc.* **2013**, *135*, 16062. (d) Yi, S.; Brega, V.; Captain, B.; Kaifer, A. E. *Chem. Commun.* **2012**, *48*, 10295.

(19) (a) Ma, S.; Smulders, M. M. J.; Hristova, Y. R.; Clegg, J. K.; Ronson, T. K.; Zarra, S.; Nitschke, J. R. *J. Am. Chem. Soc.* **2013**, *135*, 5678. (b) Neelakandan, P. P.; Jimenez, A.; Nitschke, J. R. *Chem. Sci.* **2014**, *5*, 908. (c) Bolliger, J. L.; Belenguer, A. M.; Nitschke, J. R. *Angew. Chem., Int. Ed.* **2013**, *52*, 7958. (d) Young, M. C.; Holloway, L. R.; Johnson, A. M.; Hooley, R. J. *Angew. Chem., Int. Ed.* **2014**, *53*, 9832.

(20) Albrecht, M.; Shang, Y.; Hasui, K.; Gossen, V.; Raabe, G.; Tahara, K.; Tobe, Y. *Dalton Trans.* **2012**, *41*, 9316.

(21) Bilbeisi, R. A.; Clegg, J. K.; Elgrishi, N.; de Hatten, X.; Devillard, M.; Breiner, B.; Mal, P.; Nitschke, J. R. *J. Am. Chem. Soc.* **2011**, *134*, 5110.

(22) Miyaura, N.; Suzuki, A. *Chem. Rev.* **1995**, *95*, 2457.

(23) (a) Stang, P. J.; Olenyuk, B.; Muddiman, D. C.; Smith, R. D. *Organometallics* **1997**, *16*, 3094. (b) Saalfrank, R. W.; Demleitner, B.; Glaser, H.; Maid, H.; Bathelt, D.; Hampel, F.; Bauer, W.; Teichert, M. *Chem.—Eur. J.* **2002**, *8*, 2679.

(24) Saalfrank, R. W.; Maid, H.; Scheurer, A.; Puchta, R.; Bauer, W. *Eur. J. Inorg. Chem.* **2010**, *2010*, 2903.

(25) Beissel, T.; Powers, R. E.; Parac, T. N.; Raymond, K. N. *J. Am. Chem. Soc.* **1999**, *121*, 4200.

(26) (a) Meng, W.; Clegg, J. K.; Thoburn, J. D.; Nitschke, J. R. *J. Am. Chem. Soc.* **2011**, *133*, 13652. (b) Clegg, J. K.; Cremers, J.; Hogben, A. J.; Breiner, B.; Smulders, M. M. J.; Thoburn, J. D.; Nitschke, J. R. *Chem. Sci.* **2013**, *4*, 68.

(27) (a) Ahlrichs, R.; Bär, M.; Häser, M.; Horn, H.; Kölmel, C. *Chem. Phys. Lett.* **1989**, *162*, 165. (b) Sierka, M.; Hogekamp, A.; Ahlrichs, R. *J. Chem. Phys.* **2003**, *118*, 9136. (c) Häser, M.; Ahlrichs, R. *J. Comput. Chem.* **1989**, *10*, 104. (d) Treutler, O.; Ahlrichs, R. *J. Chem. Phys.* **1995**, *102*, 346. (e) Von Arnim, M.; Ahlrichs, R. *J. Comput. Chem.* **1998**, *19*, 1746.

(28) (a) Perdew, J. P.; Burke, K.; Ernzerhof, M. *Phys. Rev. Lett.* **1996**, *77*, 3865. (b) Grimme, S.; Antony, J.; Ehrlich, S.; Krieg, H. *J. Chem. Phys.* **2010**, *132*, 154104.

(29) Binkley, J. S.; Pople, J. A.; Hehre, W. J. *J. Am. Chem. Soc.* **1980**, *102*, 939.

(30) (a) Weigend, F.; Ahlrichs, R. *Phys. Chem. Chem. Phys.* **2005**, *7*, 3297. (b) Weigend, F. *Phys. Chem. Chem. Phys.* **2006**, *8*, 1057.

(31) (a) Clegg, J. K.; Li, F.; Jolliffe, K. A.; Meehan, G. V.; Lindoy, L. F. *Chem. Commun.* **2011**, *47*, 6042. (b) Scherer, M.; Caulder, D. L.; Johnson, D. W.; Raymond, K. N. *Angew. Chem., Int. Ed.* **1999**, *38*, 1587.

(32) (a) Nakamura, T.; Ube, H.; Miyake, R.; Shionoya, M. *J. Am. Chem. Soc.* **2013**, *135*, 18790. (b) Kishi, N.; Akita, M.; Yoshizawa, M. *Angew. Chem.* **2014**, *126*, 3678. (c) Canevet, D.; Pérez, E. M.; Martín, N. *Angew. Chem., Int. Ed.* **2011**, *50*, 9248. (d) Sánchez-Molina, I.; Grimm, B.; Krick Calderon, R. M.; Claessens, C. G.; Guldi, D. M.; Torres, T. *J. Am. Chem. Soc.* **2013**, *135*, 10503.

(33) Peaks for the S_4 isomer of [$C_{70} \subset$ **1**] could not be clearly identified due to their low intensity and are not marked. We estimate this isomer accounts for ca. 5% of the total distribution.
(34) Semenov, K. N.; Charykov, N. A.; Keskinov, V. A.; Piartman, A. K.; Blokhin, A. A.; Kopyrin, A. A. *J. Chem. Eng. Data* **2009**, *55*, 13.
(35) Kleywegt, G. J.; Jones, T. A. *Acta Crystallogr.* **1994**, *D50*, 178.
(36) Shoji, Y.; Tashiro, K.; Aida, T. *J. Am. Chem. Soc.* **2004**, *126*, 6570.
(37) Ji, Q.; Lirag, R. C.; Miljanic, O. S. *Chem. Soc. Rev.* **2014**, *43*, 1873.
(38) Friščić, T.; Lancaster, R. W.; Fábián, L.; Karamertzanis, P. G. *Proc. Natl. Acad. Sci. U.S.A.* **2010**, *107*, 13216.
(39) In some cases small shifts were observed in the guest signals. In all cases these shifts were at least an order of magnitude less than those observed when the guest was bound by cage **1**.
(40) Nowell, H.; Barnett, S. A.; Christensen, K. E.; Teat, S. J.; Allan, D. R. *J. Synchrotron Radiat.* **2012**, *19*, 435.
(41) *CrystalClear, 2.0 ed.*; Rigaku Americas and Rigaku Corporation: The Woodlands, TX, 1997−2009.
(42) Parsons, S. *ECLIPSE*; University of Edinburgh: Edinburgh, U.K., 2004.
(43) Bruker-Nonius. *APEX, SAINT and XPREP*; Bruker AXS Inc.: Madison, WI, 2013.
(44) Farrugia, L. J. *J. Appl. Crystallogr.* **1999**, *32*, 837.
(45) Palatinus, L.; Chapuis, G. *J. Appl. Crystallogr.* **2007**, *40*, 786.
(46) Sheldrick, G. *Acta Crystallogr.* **2008**, *A64*, 112.
(47) van der Sluis, P.; Spek, A. L. *Acta Crystallogr.* **1990**, *A46*, 194.
(48) Spek, A. L. *PLATON: A Multipurpose Crystallographic Tool*; Utrecht University: Utrecht, The Netherlands, 2008.
(49) Grimme, S.; Ehrlich, S.; Goerigk, L. *J. Comput. Chem.* **2011**, *32*, 1456.
(50) Eichkorn, K.; Treutler, O.; Öhm, H.; Häser, M.; Ahlrichs, R. *Chem. Phys. Lett.* **1995**, *242*, 652.